Sample title

Voltage Noise Thermometry in Integrated Circuits at Millikelvin Temperatures

G. Ridgard*,[1,2] M. Thompson,[1] L. Schreckenberg,[3] N. Deshpande,[3] A. Cabrera-Galicia,[3] O. Bourgeois,[4] V. Doebele,[4] and J. Prance[1]

[1)]*Lancaster University Physics Department, Lancaster, UK*
[2)]*Quantum Motion, London, UK*
[3)]*Integrated Computing Architectures - ICA | PGI-4,*
Forschungszentrum Jülich GmbH, 52425 Jülich, Germany
[4)]*Institut NEEL, Univ. Grenoble Alpes, Grenoble, France*

(*Electronic mail: g.ridgard@lancaster.ac.uk)

This paper demonstrates the use of voltage noise thermometry, with a cross-correlation technique, as a dissipation-free method of thermometry inside a CMOS integrated circuit (IC). We show that this technique exhibits broad agreement with the refrigerator temperature range from 300 mK to 8 K. Furthermore, it shows substantial agreement with both an independent in-IC thermometry technique and a simple thermal model as a function of power dissipation inside the IC. As the device under test (DUT) is a resistor, it is feasible to extend this technique by placing many resistors in an IC to monitor the local temperatures, without increasing IC design complexity. This could lead to better understanding of the thermal profile of ICs at cryogenic temperatures. This has its greatest potential application in quantum computing, where the temperature at the cold classical-quantum boundary must be carefully controlled to maintain qubit performance.

I. INTRODUCTION

At deep cryogenic temperatures (< 4 K), power dissipation in electronic components can induce significant localised heating[1]. The primary cause is the reduction in the thermal conductivity of both silicon[2] and the insulating materials in its packaging[3], coupled with the increase of the thermal boundary resistances[4]. This issue is particularly important in Quantum Information Processing (QIP). The optimal performance of many types of qubit[5–7] occurs at deep cryogenic temperatures due to diminished thermal noise. These qubits require ancillary classical electronics for control and read-out. As the qubit count scales, so does the requisite number of wires. To mitigate the unsustainable proliferation of wires into the cryostat, additional classical electronics are now co-located with the quantum components[8,9]. Consequently, monitoring the local temperature at the qubit-classical electronics interface becomes crucial for maintaining consistent qubit operation.

While thermometry at deep cryogenic temperatures has been studied for many years, some existing solutions are inadequate for determining the temperature within an integrated circuit (IC). The most prevalent thermometry technique, temperature coefficient of resistance (TCR) thermometry[10–12], is unsuitable because the thermometer will be poorly thermalised to the IC interior due to the low thermal conductivity of silicon and the thermal boundary resistance between the IC and the thermometer. Thermometry methods have been developed for use within ICs to address this issue[13,14]. Methods such as Gate Resistance Thermometry (GRT)[15,16], quantum dot thermometry[17–19], and diode thermometry[20,21] each have their individual merits and specific applications, but all have associated power dissipation inside the IC. Consequently, all will influence the internal temperature of the IC.

One such technique which is both dissipationless and primary is noise thermometry[22]. This has been well established in a broad range of environments[23–26]. However, it has several barriers to entry as a technique for measuring the internal temperature of an IC at temperatures that QIP platforms are located. The first problem is that in the case of voltage noise thermometry the device under test (DUT) resistor must have a very high resistance to make the noise measurable above the typical readout amplifier noise. High resistance values result in low cut off frequencies, making measurements extremely slow and susceptible to 1/f noise. This paper demonstrates the use of the cross-correlation technique to remedy this issue. Cross-correlation allows the use of lower value resistors by allowing the measurement of noise values below the noise of the amplifiers used in the setup. In this paper we demonstrate this by using cross-correlation to accurately measure the temperature of our DUT, a 45 kOhm resistor, from 300 mK to 8 K.

Another problem in performing noise thermometry in an IC is the potential for non-thermal noise contributions. The resistors are typically made of doped silicon, which as a semiconductor has many more potential sources of noise[27] and the close proximity of power dissipating devices (on the order of 100 μm) may provide a source of cross-talk in the spectral measurements. In this paper, we resolve this problem by showing that even if the resistors have non-thermal noise sources, if this is appropriately characterised then its contribution can be subtracted from the spectral measurements, enabling accurate noise thermometry. We demonstrate this by first showing that our DUT has an elevated noise level at the fridge base temperature, which cannot be attributed to thermal noise. Next, from the base temperature measurement, we extract an offset noise (the non-thermal contribution). We then calibrate the noise temperature against the refrigerator temperature. It was found that when the offset noise is subtracted from the spectral measurements, the noise thermometry shows good agreement with the temperature of the refrigerator from
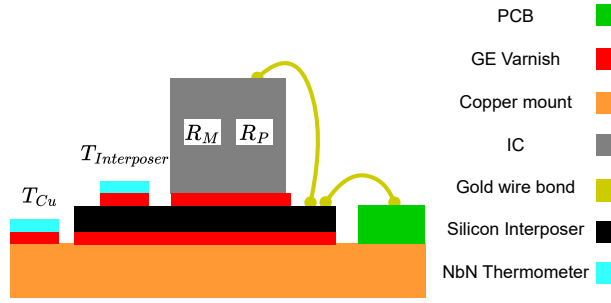
FIG. 1. Illustration of the setup: PCB board composed of standard FR4. The GE varnish was lightly diluted to aid its application. The copper mount was constructed from a 6 mm thick piece of C110 oxygen free copper which has a minimum of 99.99 % purity. The silicon interposer was $550\mu m$ thick and was lightly boron doped with gold patterned on top to allow for bonding between IC, interposer and PCB. Two Niobium Nitride (NbN) based thermometers were placed on the copper and silicon interposers to monitor their temperature as a function of power. Details on their operation and calibration can be found in Appendix C. This illustration is not to scale.

300 mK to 8 K. This was further tested by comparing the noise temperature against a different in-IC thermometry technique (TCR of the resistor) as a function of power.

In Sec II, we present our measurement setup and protocol of voltage noise thermometry inside an IC. Next, in Sec III, we examine the noise characteristics of the resistor selected for the experiment and its calibration against the temperature of the Mixing Chamber (MXC) in a refrigerator. Finally, we compare this technique to another internal thermometry method and a thermal model in Sec IV.

II. SET UP

Figure 1 illustrates the IC configuration. The IC, a 2 mm x 2 mm x 0.8 mm chip, is affixed to a silicon interposer, mounted on a ultra-high-purity copper mount, which in turn is secured to the puck connected to the MXC. The device is interconnected via gold bond wires to gold traces on the interposer, and subsequently bonded to the printed circuit board (PCB). The IC contains a 350 Ω power resistor, R_P, and a 45 kΩ measurement resistor, R_M. These components are fabricated using an industrial 65 nm bulk CMOS process. The entire assembly is cooled by an *Oxford Instruments Triton 400* dilution refridgerator.

A. Measurement Principle

For a resistor with resistance R_M at a temperature T, the Johnson-Nyquist theorem[28,29] states that the power spectral density, S_D^2, within a 1Hz bandwidth across the resistor is expressed as

$$S_D^2 = 4k_B T R_M \quad \left[\frac{V^2}{Hz}\right]. \tag{1}$$

Consequently, if the resistance is precisely known, the resistor can serve as a primary thermometer, with the temperature determined by

$$T = \frac{S_D^2}{4k_B R_M}. \tag{2}$$

To determine S_D^2, we calculate a cross-correlated spectrum to measure noise levels beneath the intrinsic noise of the amplifiers[30,31]. This demands the simultaneous acquisition of voltage as a function of time via two amplifier channels. The time traces of amplifiers α and β, denoted as $V_\alpha(t)$ and $V_\beta(t)$ respectively, contain a shared signal, $V_C(t)$, alongside a noise component pertinent to the input noise of each amplifier, $V_{\alpha:n}(t)$ and $V_{\beta:n}(t)$. In this context, $V_C(t)$ represents the thermal voltage originating from the resistor. The expressions for the amplifier signals are given by,

$$V_\alpha(t) = V_C(t) + V_{\alpha:n}(t), \tag{3}$$

and

$$V_\beta(t) = V_C(t) + V_{\beta:n}(t). \tag{4}$$

Each cross-correlation spectrum, S_{cc}^2, is derived by computing the dot product of the Fourier transform of one trace with the complex conjugate of the Fourier transform of the other,

$$S_{cc}^2(f) \rightarrow \tilde{V}_\alpha(t)^* \cdot \tilde{V}_\beta(t). \tag{5}$$

The resultant spectrum are then averaged n times to attenuate uncorrelated noise, yielding $\langle S_{cc}^2(f) \rangle_n$. With adequate averaging, this converges to the Fourier transform of the common signal,

$$\langle S_{cc}^2(f) \rangle_n = \tilde{V}_C(f). \tag{6}$$

Given the complex nature of this spectra, its magnitude is computed and subsequently scaled to account for the windowing effect during the Fourier transform. Finally, the average value over a frequency range $f_1 - f_2$ encompassing m points is calculated to produce our final value,

$$S_D^2 = \frac{1}{m} \sum_{i=f_1}^{f_2} |\langle S_{cc}^2(f_i) \rangle_n| \tag{7}$$

which is then converted to an Equivalent Noise Temperature (ENT) by Eq.2.

B. Detail of operation

A diagram of the electrical set up of the experiment is given in Fig. 2. The time traces in our experiment were recorded using two *Zurich Instruments MFLIs* . Both amplifiers were synchronized and triggered via the Multi-Device Synchronization (MDS) package. To ensure the simultaneity of the traces, measurement timestamps from each amplifier were compared, ensuring that the traces commenced within a maximum of 20 μs. The amplifiers acquired data at $f_{clock}/2^9 \approx 120$ kHz,
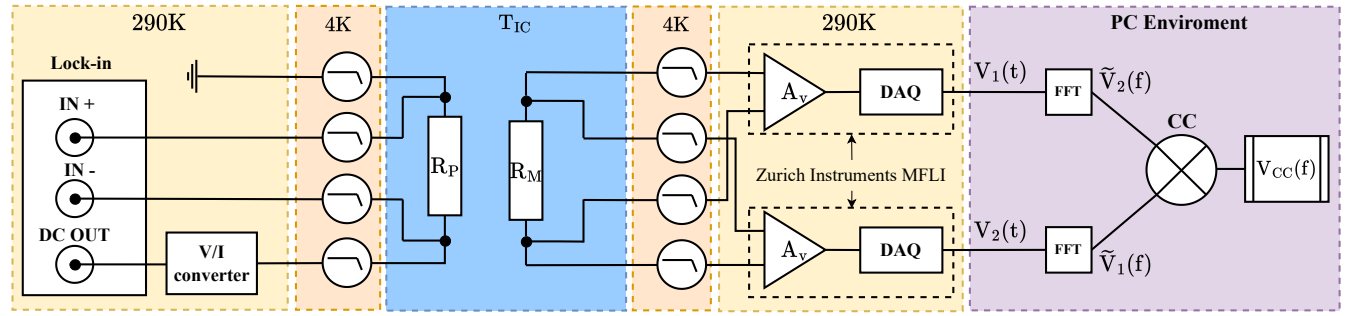
FIG. 2. Experiment Schematic: The first box on the left side contains a *Zurich Instruments MFLI* lock-in amplifier which provides a DC voltage through the auxiliary output to a *Lancaster University*-designed low noise voltage-current converter, which converts at $1\mu A/V$. This drives a current through the power resistor R_P. The same MFLI then measures the corresponding voltage response by demodulating at 0 Hz. The power through R_P and as such in the IC is then given by the product of the DC current and DC voltage response. All lines down to low temperature are filtered at the 4 K plate by *Aivon* Low Pass Filters (LPF). The next box shows the power resistor R_P and the measurement resistor R_M in the IC at a temperature T_{IC}. The resistors are separated by 221 μm in the IC. Finally, R_M is connected to two MFLIs that provide simultaneous voltage readings across the resistor. Finally, both voltage time series are then Fourier transformed and have the cross-spectrum calculated by a Python script.

where f_{clock} denotes the clock frequency of 60 MHz, collecting 2^{16} samples. This configuration results in a measurement duration of 0.56 s per spectrum. Following the acquisition of both time traces, the cross-correlation spectrum was computed to attenuate non-correlated noise. This spectrum was subsequently averaged to further reduce residual noise. In our study, the number of averages was set to 3000, a value selected to limit the total measurement time to under 30 minutes. The requisite number of averages to sufficiently attenuate the measurement-specific noise floor is a function of both the noise, α, (in $V/\sqrt{Hz}$) of a single channel amplifier, and the noise floor targeted for resolution, γ. The number of averages to achieve a ratio of unity between the expected standard deviation of the measured value and the expected measured value is determined by

$$n = \frac{1}{2\gamma^4}\left[(\alpha^2 + \gamma^2)^2 + \gamma^4\right] \qquad (8)$$

which follows Rubiola[32] but conserves the contribution of the amplifier noise. This relationship can also be found derived in[33], its link to the variance in measurements of noise power is further explored in Appendix A. Considering the number of averages and that at low frequencies the noise floor of a single channel is approximately 4 nV/$\sqrt{Hz}$, we can re-arrange Eq.8 to derive the minimum measurable noise floor,

$$\gamma^2 = \frac{\alpha^2}{\sqrt{2n-1}-1}. \qquad (9)$$

This yields $\gamma \approx 0.5\,nV/\sqrt{Hz}$, corresponding to a minimum measurable temperature of approximately 100 mK (for $R = R_M = 45\,k\Omega$). Conversely, in the absence of cross-correlation, the minimum resolvable noise would be that of the amplifier at low frequencies, with an equivalent minimum temperature of ≈ 6.4 K. Five distinct frequency ranges were selected to compute an average spectral density. These ranges were determined by examining the base temperature spectra and identifying regions without frequency peaks generated from interference from other electrical sources.
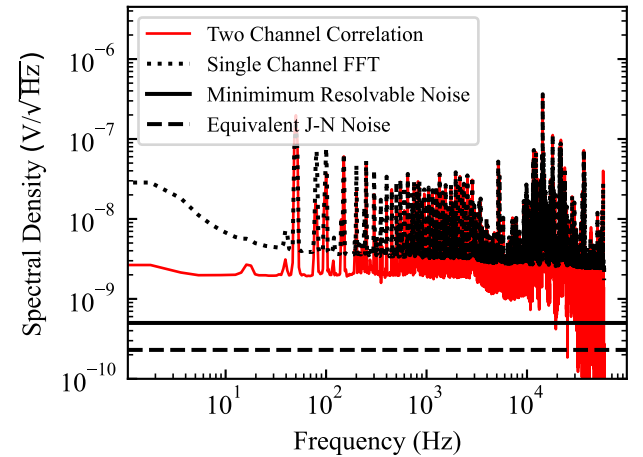

FIG. 3. Base Temperature Measurement of R_M after 3000 spectral averages. We see that the correlation is working as the two channel correlation (red line) is below that of the single channel FFT (dotted line). However, the two channel correlation should be much closer to the minimum resolvable noise (black line) as the thermal contribution at base (dashed line) is below the minimum resolvable noise. Therefore there must be another source of noise, other than the thermal contribution.

C. Characterisation of measurement resistor

Preliminary noise measurements at a base temperature of T = 15 mK indicated that the measurement resistor exhibited an anomalously elevated noise floor, as depicted in Fig. 3. Although this noise level is lower than that of the amplifier, it possesses an ENT of 1.77 K. To ascertain that this observation was not an artifact of the experimental configuration, noise measurements across the resistor were also conducted in an alternative section of the setup (R = 9 kΩ) and with a dead short of the measurement resistor, as illustrated in Fig. 4. Both

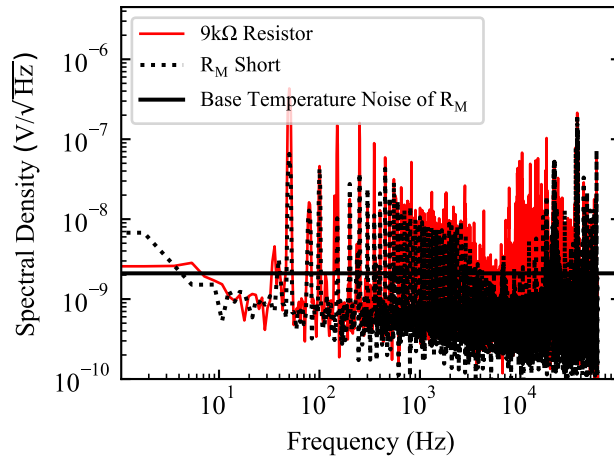FIG. 4. Base Temperature measurements of R_M shorted and a 9 kΩ resistor: Here we see the two channel correlation of both the shorted R_M and the 9 kΩ resistor are much below the noise floor of the base temperature measurement of R_M. This rules out the offset noise associated with R_M being related to the set up.

of these values are below the noise level of the measurement resistor at base temperature. This indicates that this excess noise is related to the measurement resistor and not the set up. We consider two options for the existence of this unexpectedly high noise level.

1. R_M does not thermalise with the MXC and instead saturates at the ENT of 1.77K.

2. The noise is caused by a combination of the base temperature thermal contribution and a constant offset from the properties of the resistor itself.

Figure 5 illustrates the resistance of R_M as a function of temperature. This was determined through four-terminal lock-in measurements with an AC current excitation of 500 pA (giving a power dissipated in the resistor of 11.3 fW, limiting the chances of the resistor overheating) at a frequency of 66 Hz, with 11 values recorded per temperature step and subsequently averaged. The absence of a resistance plateau at the noise equivalent temperature of 1.77 K implies that at these temperatures, the resistor remains thermalised to the MXC rendering scenario 1 unlikely. The precise origin of the noise was challenging to determine due to the unknown construction of the resistor. However, literature has shown that non-thermal noise is prevalent in silicon-based resistors at low temperature[34]. We consider this noise (denoted by $S_{Offset}(f)$) to be temperature independent, thus treating it as an offset that can be subtracted from our correlated spectral values. To calculate this value, we take the a spectral measurement of the resistor at a well-defined temperature, measure the resistance and then subtract the theoretically predicted Johnson-Nyquist value at this temperature. In practice this is performed at base temperature so to minimise the impact of error from the thermal noise contribution on the eventual noise offset value. The temperature at base was 15 mK based on the MXC thermome-
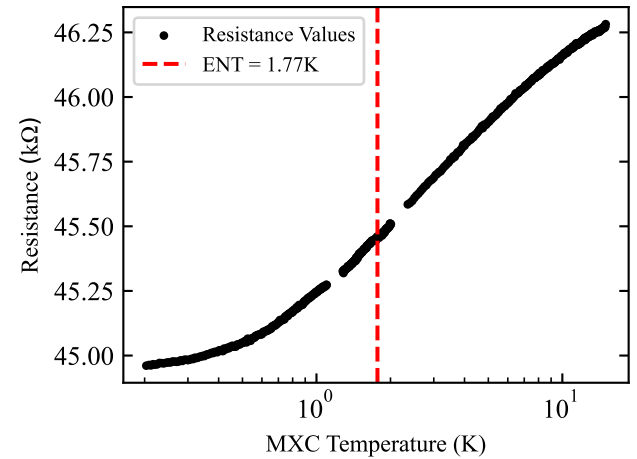

FIG. 5. Resistance of R_M as a function of temperature: The resistance of R_M continues to change past the ENT of the base temperature noise measurement. This would suggest that R_M is still thermalised to the MXC plate and hence would rule out that the saturation in the temperature of R_M as the source of the extra noise.Breaks in resistance measurement data at around 1 K and 2 K are due to He3-He4 mixture instabilities, meaning the PID temperature controller struggles to stablise the temperature. At around 1 K the mixture separates into separate He3 and He4 phases and at 2.17 K He4 undergoes a phase change (the lambda transition).

ter reading. The theoretical base temperature contribution, $S_{T=15mK}$, was calculated using this temperature and a resistance reading. The total spectral density at base after sufficient cross correlation averages, $\langle S^2_{Base}(f)\rangle$, is given by,

$$\langle S^2_{Base}(f)\rangle = S^2_{Offset}(f) + S^2_{T=15mK}. \quad (10)$$

For the average spectra at every temperature step, x, $\langle S_{MXC=x}(f)\rangle$, we remove $S_{Offset}(f)$, with the result $S_{T=x}(f)$,

$$\langle S^2_{T=x}(f)\rangle = \langle S^2_{MXC=x}(f)\rangle - S^2_{Offset}(f), \quad (11)$$

which is then converted into a ENT by averaging the values in a range of white noise frequencies.

III. NOISE TEMPERATURE VS MXC TEMPERATURE

In order to verify noise thermometry we compared the noise temperature of the resistor against the MXC thermometers. We increased MXC from 100 mK to 8 K in twelve steps. At each temperature step the resistance was measured to ensure its value was well known. At each step spectra were recorded, processed and averaged according to Sec. II. The results of this experiment are shown in Fig. 6. Further details on the agreement with the MXC temperature is provided in Fig. 7. Although the noise temperature generally aligns with the MXC temperature, it is only beyond 200 mK that the measured values begin to fall within the uncertainties of the MXC temperature. The uncertainty in the noise temperature also encompasses the uncertainty arising from the offset noise
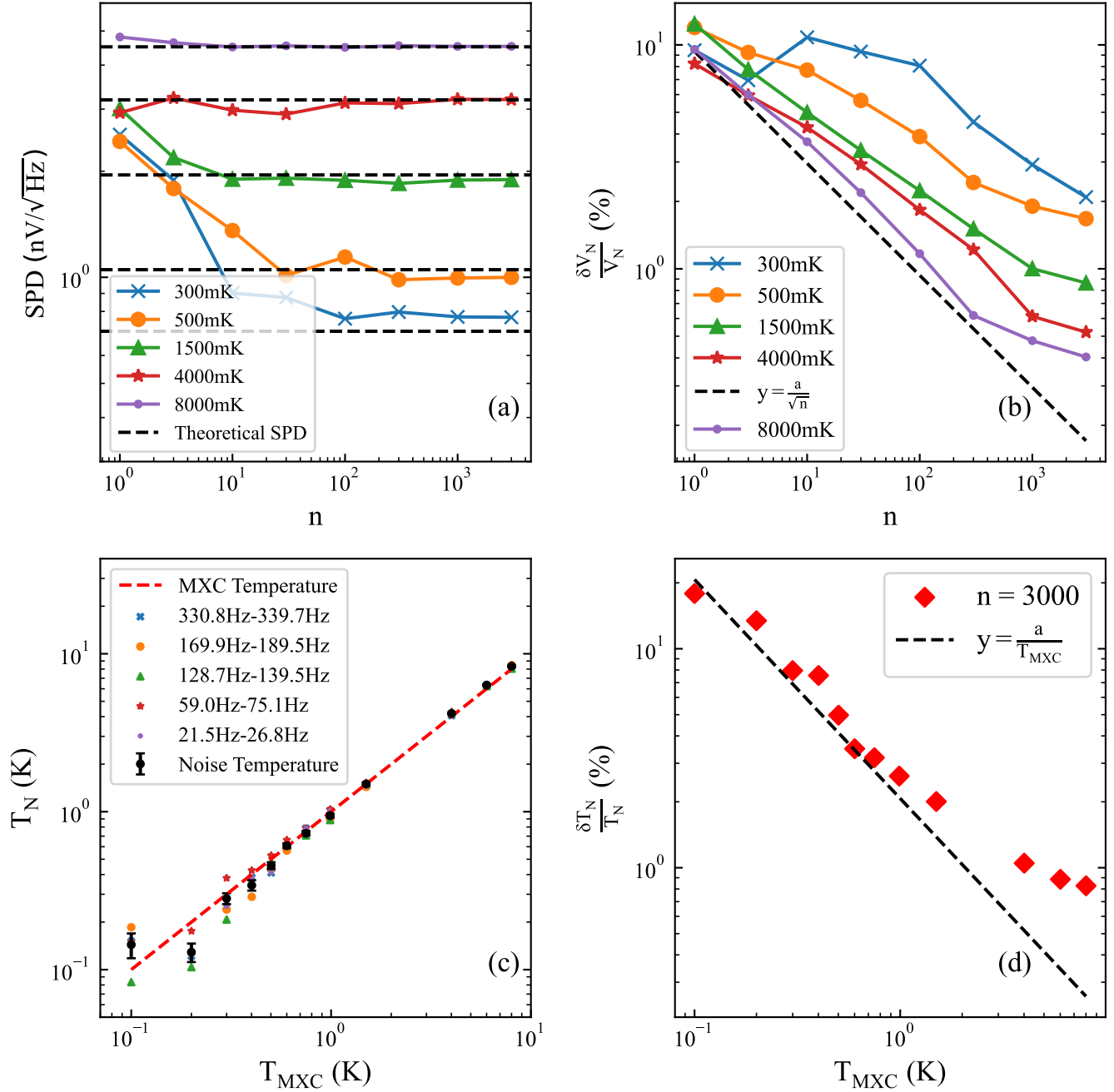
FIG. 6. a) Measured Spectral density (SPD) as a function of the number of averages for various temperature ranges: At lower temperatures, increased averaging is required to sufficiently attenuate non-correlated noise and achieve the theoretical value. The theoretical SPD is derived from the Johnson-Nyquist formula, using the MXC temperature and a measured resistance value of R_M. b) Relative error in the SPD value as a function of the number of averages: The relative error is shown to be inversely proportional to the square root of the number of averages. This relationship begins to deteriorate at higher values of n, due to the inclusion of the error in the offset spectral density value, which remains constant. c) Noise temperature versus MXC temperature: Different-shaped markers represent the average values in various frequency ranges as indicated in the legend. The black points denote the average value across all frequency ranges at each temperature. This plot indicates that the noise temperature agrees in general with the MXC temperature. d) Relative error in temperature versus MXC temperature: This plot illustrates that the relative error in temperature is inversely proportional to the temperature, assuming that the Johnson-Nyquist SPD target noise is significantly lower than the SPD of the amplifier channel input. At elevated temperatures, this relationship deteriorates.Each data point here contains all of the contributions from each of the frequency bins.
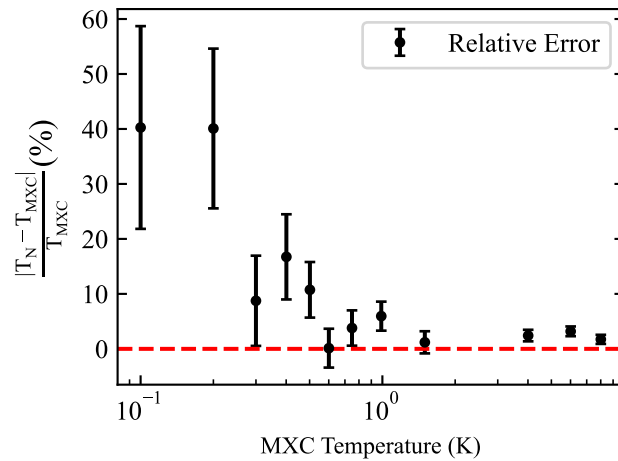
FIG. 7. Relative error of the noise thermometry against the mixing chamber. The error bars are calculated from the standard error in the spectral measurements at these temperature values. Deviation from the MXC temperature can be expected to increase at lower temperatures, as it takes many more averages for the cross correlation to converge. If this doesn't converge properly, then the temperature will be incorrectly estimated as the contributions from the amplifier noise won't have been sufficiently attenuated. The relative error also increases at lower temperature, as outlined in Appendix A.

value. Therefore, employing a resistor without an offset will reduce the uncertainty across all temperature ranges. Additionally, due to the presence of noise offset, this method no longer qualifies as a form of primary thermometry. This is predicated on the assumption that the R_M thermalises at the base temperature of 15 mK, an assumption that cannot be verified with certainty. Nonetheless, at temperatures exceeding 2 K, the impact of this assumption constitutes less than 1 % of the total value, rendering its effect almost negligible.

The principal limitation of this methodology is that the relative uncertainty is inversely proportional to the square root of the number of averages and inversely proportional to the temperature of the resistor. This in essence, is derived from making an estimate of a random variable (the temperature) from a finite sample (the voltage spectra), which is essentially the Rice relationship (explicit links are discussed further in Appendix A). For instance, with 3000 averages, to achieve a relative uncertainty of less than 2%, the maximum measurable temperature is approximately 1.5 K. Alternatively, limiting measurement time to 1 minute requires 100 averages. For a relative uncertainty of 2% this is limited to approximately 8 K or greater. Consequently, the primary constraint of this technique is the extended duration required for averaging to achieve lower temperatures and reduced relative uncertainties. The main solutions to this problem can be summarised as:

1. Lower the input noise of the amplifiers.

2. Decrease the time it takes to acquire one spectrum.

One such alternative set up would be the use of cryo-amps. The lower noise floor of the amplifiers would allow a lower resistance value to be used; this would, in turn, increase the cutoff frequency of the RC circuit created by the resistor and parasitic wire capacitance. A higher cut-off frequency would allow for a higher sampling rate and reduce the time per spectral acquisition. A good example of accurate high frequency noise thermometry would be Crossno et al[35].

IV. NOISE TEMPERATURE VS POWER DISSIPATION

To substantiate noise thermometry, it was important to conduct *in situ* testing by applying power within the IC while simultaneously measuring the temperature. This validation step is crucial, as the proximity of a power-dissipating element to R_M could potentially induce cross-talk, thereby compromising the accuracy of noise measurements. To validate the noise thermometry, we utilised an alternative in-IC methodology, specifically the TCR technique that employs R_M. We used the temperature dependence characterised in Fig. 5 as a calibration reference against the MXC. Initially, we tested TCR thermometry in relation to power dissipation ranging from 600 nW to 100 μW. This was to ensure the temperature was larger than 300 mK, at which temperatures the both the noise thermometer and TCR was considered to be accurate. At each increment, resistance measurements were taken and subsequently converted to temperature using the established calibration. Subsequently, to assess the noise thermometry, power was applied at seven levels, and at each level the spectra were processed and averaged in accordance with the methodology outlined in Sec. II. A baseline spectrum was recorded with the power resistor connected but without power dissipation to re-calibrate the offset spectral density. This was done to account for any potential cross-talk from the power resistor that might be present in all measurements.

The temperature inside the IC can be modelled in the idealised case that we consider the power source to be a point source at the centre of the top surface of the IC. We then consider the heat propagation to be radial from the heat source. We next have to consider, l, the mean free path of phonons within the silicon. This value is not well-defined but can be large (on the order of centimeters[4]) in pure silicon at low temperatures. If l approaches the characteristic length scale of the phonon container (L, in our case 2 mm) then the heat equation breaks down. This is because generating a temperature gradient requires multiple phonon scattering events throughout the length that is defined to have a gradient. In this case phonons are considered to behave ballistically, and the Boltzmann Transport Equation is more suited to describing the temperature profile[36]. However, in ICs there are many places to provide scattering events. In the case of substrates with high dopant concentrations, this could be the dopant centers. Another place for scattering events is the top layer of the IC, which contains many different types of materials, which at low temperature can cause phonon mismatch at the boundaries and therefore scattering. The Knudsen number (Kn) helps to determine the boundary between ballistic and diffu-

sive energy carrier propagation[37] and is defined as

$$Kn = \frac{\Lambda}{L}. \tag{12}$$

It gives the ratio between the characteristic distance an energy carrier travels (Λ) and the characteristic length scale of the system (L). In our case

$$Kn = \frac{l}{L}. \tag{13}$$

If $Kn \leq 0.1$, we can consider the system to act diffusively. If we use the diffusive model then the corresponding steady state heat equation is given by,

$$\frac{1}{r^2} \frac{\partial}{\partial r} \left(r^2 \alpha T^3 \frac{\partial T}{\partial r} \right) = 0, \tag{14}$$

with the conductivity, $\kappa = \alpha T^3$. For silicon, this expression can be given by[4,38],

$$\kappa(l) = \alpha T^3 = 1200 l T^3. \tag{15}$$

Equation 14 does not contain a source term as its assumed all of the heat is dissipated back into the MXC. To solve it, several boundary conditions are given; the first is,

$$r = R, \quad T = T_{Interposer}(Q) \tag{16}$$

where $T_{Interposer}(Q)$ is the temperature of the silicon interposer at a given power. R in our case is the distance from the power source to the silicon interposer, which is 1 mm. Interestingly, the temperature of the interposer greatly exceeds the copper holder and the MXC temperature (see Appendix D) due to the large boundary resistance at the copper - varnish - interposer boundary. Next,

$$r \to 0, \quad \alpha T^3 \frac{\partial T}{\partial r} = \frac{Q}{2\pi r^2}. \tag{17}$$

This boundary condition states that the heat flux is equal to the total power dissipated (Q) divided by the area of hemisphere created by the radial movement of heat from the top surface. The solution to this equation is then,

$$T = \left[\frac{2Q}{1200\pi l} \left(\frac{1}{r} - \frac{1}{R} \right) + T_{Interposer}^4(Q) \right]^{\frac{1}{4}}, \tag{18}$$

where $r = 221\mu$m. The results of both TCR, noise thermometry and Eq. 18 fitted for l are illustrated in Fig. 8. Both data sets exhibit reasonable degree of agreement, thereby substantiating the efficacy of noise thermometry across a range of power dissipation levels. However, variation in the different frequency bins at each measurement point suggests that this technique would be improved by increasing the number of point averaged, to average out this variation. These findings imply that this methodology could be suitable for application within ICs containing multiple power-consuming devices.
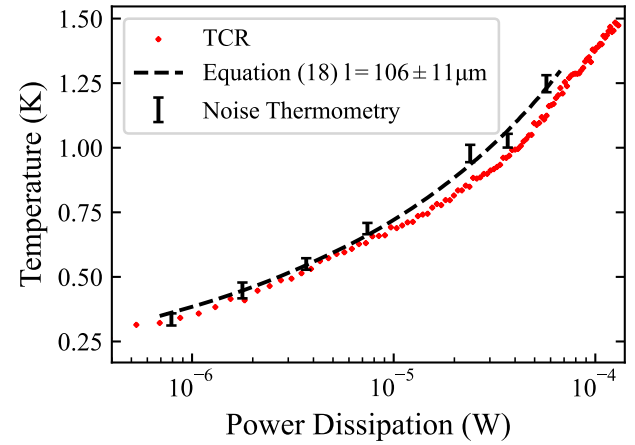

FIG. 8. Temperature Coefficient of Resistance Thermometry (TCR) of R_M and Noise Thermometry as a Function of Power: Noise thermometry agrees broadly with the TCR, but typically exceeds it. This could be explained through two scenarios. The first is that the baseline offset for the noise thermometry was slightly too large, possibly through the device not being properly thermalised to the MXC during its measurement. Secondly, if the TCR calibration was performed too quickly, it could also be suffering from a slight temperature offset. The dashed line fit fits Eq.18 to the noise data and gives an estimate of $l = 106 \pm 11\mu$m (under the assumption that l is either constant or weakly temperature dependent in the range of interest) which means that $Kn \approx 0.1$. This fit suggests a diffusive model is still appropriate.

V. CONCLUSIONS

We have established that noise thermometry exhibits broad agreement with other thermometry in the range 300 mK to 8 K. Furthermore, it shows substantial agreement the predicted temperature, when employed to determine the IC temperature corresponding to a specific power dissipation. This form of thermometry was made to be effective by the use of both cross-correlation and the subtraction of the offset noise calculated from base temperature measurements. This work suggests that with the addition of these techniques, voltage noise thermometry could be broadly applicable to ICs developed with industrial CMOS processes. However, the offset noise does preclude the noise thermometry in this paper from being a primary method of thermometry. Employing a resistor devoid of additional noise would reduce the measurement uncertainties and retain the technique as a primary thermometry method. The presence of non thermal noise in this setup also re-enforces the need for repeated experiments on different types of resistors, to fully demonstrate the efficacy of this approach. Although this work demonstrates the increase in the uncertainty of measurements at lower temperatures and the large measurement time, we describe how the use of cold amplifiers could rectify both of these issues. Furthermore, as the direction of quantum computing moves towards temperatures closer to 1 K to access higher cooling power[39–42], this method will require less averaging to attenuate uncorrelated noise. This will mean faster measurements and lower uncertainties.

Journal of
Applied Physics

AIP
Publishing

In addition, the implementation of this technique is straight-forward and requires only standard instruments that are typically available in academic or commercial laboratories. Given that the devices used are only resistors, this method significantly reduces the time and resources required for the design of ICs, facilitating the placement of thermometers at multiple locations within an IC. Finally, we suggest that this technique is an excellent candidate for performing in-IC temperature measurements to map the thermal profile of operational quantum-classical circuitry because of its dual primary and dissipationless nature.

VI. ACKNOWLEDGMENTS

VII. CONFLICT OF INTEREST STATEMENT

The authors have no conflicts to disclose

VIII. APPENDIX

A. Uncertainty in Temperature

The expectation relative error in the spectral measurement $\frac{\delta S}{S}$, the ratio of the expected standard deviation to the expected spectral value, is calculated from[32]. This is a function of the amplifier channels' power spectral density, A^2, the target noise level, X^2, and the number of averages, n, we can look at how the relative error changes with temperature within our measurements. As,

$$\frac{\delta S}{S} = \frac{1}{X^2}\sqrt{\frac{(A^2+X^2)^2+X^4}{2n}}, \tag{1}$$

and we know that $S \propto T$ then it follows that in the case that the relative error in the resistance is small, that,

$$\frac{\delta T}{T} \propto \frac{1}{X^2}\sqrt{\frac{(A^2+X^2)^2+X^4}{2n}}. \tag{2}$$

In the low temperature case, where $X^2 \ll A^2$, this expression simplifies further,

$$\frac{\delta T}{T} \propto \frac{1}{\sqrt{2n}}\left(\frac{A^2}{X^2}+1\right). \tag{3}$$

We know that in our case $X^2 = 4k_BTR$ in a 1Hz bandwidth and that A^2 is constant with temperature. As such, we can say,

$$\frac{\delta T}{T} \propto \frac{1}{T\sqrt{2n}}. \tag{4}$$

Here, the $1/\sqrt{n}$ relationship represents the contribution of the, Rice relationship, usually given by

$$\frac{\sigma_Y}{Y} = \frac{1}{\sqrt{\Delta t \Delta f}}. \tag{5}$$

Where σ_Y is the standard deviation of some Gaussian variable Y, Δt is the time spent measuring, and Δf represents measurement bandwidth. Equation 1 converges to the Rice relationship when firstly, we note that

$$n = \tau f_C \tag{7}$$

where τ is our total integration time and f_C is the correlation bandwidth. Secondly, if we take the amplifier noise to zero, we recover the Rice relationship

$$\frac{\delta S}{S} = \frac{1}{X^2}\sqrt{\frac{2X^4}{2n}} = \frac{1}{\sqrt{n}} = \frac{1}{\sqrt{\tau f_C}} \equiv \frac{1}{\sqrt{\Delta t \Delta f}}. \tag{8}$$

B. Uncertainty in Noise Temperature

Given the Johnson-Nyquist relationship between temperature and spectral density given in Eq. 2 the relative uncertainty in temperature, $\frac{\delta T}{T}$, is given by,

$$\frac{\delta T}{T} = \sqrt{\left(\frac{\delta S_D^2}{S_D^2}\right)^2 + \left(\frac{\delta R}{R}\right)^2}. \tag{9}$$

In this experiment, δR is given by the standard error of the resistance measurements taken at every temperature step, while R is given by the average value. For the spectral density, δS_D^2 is taken from the standard error of the values of the frequency values chosen to be averaged. However, because we have to remove an offset at each step, we need to take this into account. As

$$S_D^2 = S_M^2 - S_{offset}^2, \tag{10}$$

where S_M^2 is the measured spectral density and S_{offset}^2 is the offset spectral density. We calculate S_{offset}^2 by,

$$S_{offset}^2 = S_{Base}^2 - S_{T=15mK}^2 \tag{11}$$

where S_{Base}^2 is the base temperature measurement and $S_{T=15mK}^2$ is the Johnson-Nyquist value of the spectral density of the resistor at 15mK, assuming the resistor is well thermalised with the MXC. The only error in $S_{T=15mK}^2$ is the error of the resistance at base in this case,

$$\delta S_{offset}^2 = \sqrt{\left(\delta S_{Base}^2\right)^2 + \left(S_{T=15\ mK}^2 \frac{\delta R_{T=15\ mK}}{R_{T=15\ mK}}\right)^2}. \tag{12}$$

Now we sum the errors of S_M^2 and S_{offset}^2 in quadrature,

$$\delta S_D^2 = \sqrt{\left(\delta S_M^2\right)^2 + \left(\delta S_{offset}^2\right)^2}. \tag{13}$$
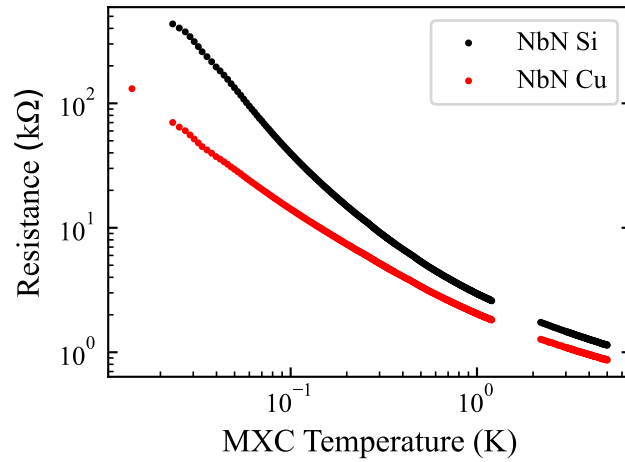
FIG. 9. NbN calibration: The MXC temperature is given by a pre-calibrated ruthenium oxide thermometer placed on the fridge mixing chamber.
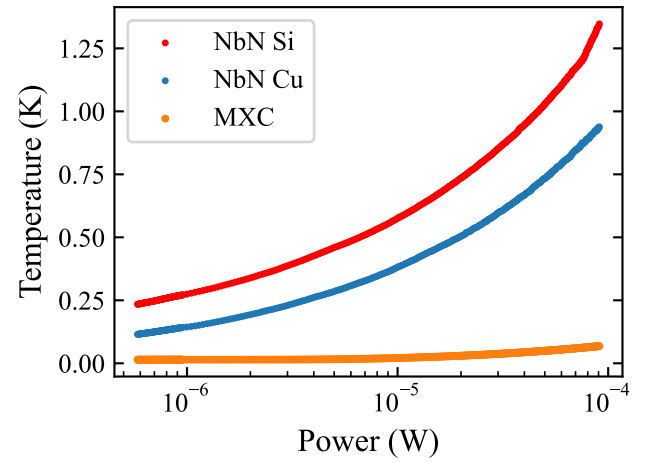

FIG. 10. Temperature of the interposer thermometer (NbN Si) and the copper thermometer (NbN Si) and mixing chamber thermometer (MXC) as a function of power applied in the IC.

C. Calibration of Niobium Nitride Thermometers

Niobium nitride thermometers were ideal candidates for monitoring both the copper and silicon interposer temperature due their excellent temperature sensitivity at milli-kevlin temperatures[44,45]. Both the interposer and copper thermometers had their resistance read out standard 4 point AC lock-in technique. The input current was 0.2 nA at 81 Hz. During the calibration, ten points were taken per temperature step, with a settling time of 3 s per point and a 3 s sweep delay. The first step to ensure adequate thermalisation was that the MXC temperature had to return two consecutive temperature readings within a defined threshold of the target temperature before it allowed the values to be taken. The temperature steps were also made to be small to further reduce the risk of poor thermalisation. From 16 mK to 360 mK the temperature step was 2 mK, from 360 mK onwards it was 5 mK. Results of the calibration are shown in Fig 9.

D. Silicon Interposer, Copper and Mixing Chamber Temperature as a Function of Power

Figure 10) demonstrates the temperature of several different thermometers at different locations on the setup. All thermometers were read out under the same conditions as their calibration.

[1]K. Blagg, A. Castagnède, and M. Singh, "On-chip heating effects in electronic measurements at cryogenic temperatures," Cryogenics **126**, 103536 (2022).

[2]C. J. Glassbrenner and G. A. Slack, "Thermal conductivity of silicon and germanium from 3 k to the melting point," Physical review **134**, A1058 (1964).

[3]J. Chawner, A. Jones, M. Noble, G. Pickett, V. Tsepelin, and D. Zmeev, "Lego® block structures as a sub-kelvin thermal insulator," Scientific Reports **9**, 1–4 (2019).

[4]E. T. Swartz and R. O. Pohl, "Thermal boundary resistance," Reviews of modern physics **61**, 605 (1989).

[5]M. Brandl, M. Van Mourik, L. Postler, A. Nolf, K. Lakhmanskiy, R. Paiva, S. Möller, N. Daniilidis, H. Häffner, V. Kaushal, *et al.*, "Cryogenic setup for trapped ion quantum computing," Review of Scientific Instruments **87** (2016).

[6]A. D. Córcoles, J. M. Chow, J. M. Gambetta, C. Rigetti, J. R. Rozen, G. A. Keefe, M. Beth Rothwell, M. B. Ketchen, and M. Steffen, "Protecting superconducting qubits from radiation," Applied Physics Letters **99** (2011).

[7]M. Veldhorst, H. Eenink, C.-H. Yang, and A. S. Dzurak, "Silicon cmos architecture for a spin-based quantum computer," Nature communications **8**, 1766 (2017).

[8]M. Gonzalez-Zalba, S. De Franceschi, E. Charbon, T. Meunier, M. Vinet, and A. Dzurak, "Scaling silicon-based quantum computing using cmos technology," Nature Electronics **4**, 872–884 (2021).

[9]S. Pauka, K. Das, R. Kalra, A. Moini, Y. Yang, M. Trainer, A. Bousquet, C. Cantaloube, N. Dick, G. Gardner, *et al.*, "A cryogenic cmos chip for generating control signals for multiple qubits," Nature Electronics **4**, 64–70 (2021).

[10]S. S. Courts, "A standardized cernox™ cryogenic temperature sensor for aerospace applications," Cryogenics **64**, 248–254 (2014).

[11]S. Courts and J. Krause, "A commercial ruthenium oxide thermometer for use to 20 millikelvin," in *AIP Conference Proceedings*, Vol. 985 (American Institute of Physics, 2008) pp. 947–954.

[12]E. Dechaumphai and R. Chen, "Sub-picowatt resolution calorimetry with niobium nitride thin-film thermometer," Review of Scientific Instruments **85** (2014).

[13]T. Huizinga, M. Babaie, A. Vladimirescu, F. Sebastiano, *et al.*, "Integrated cryo-cmos temperature sensors for quantum control ics," in *2022 IEEE 15th Workshop on Low Temperature Electronics (WOLTE)* (IEEE, 2022) pp. 1–4.

[14]G. M. Noah, T. H. Swift, M. De Kruijf, A. Gomez-Saiz, J. J. Morton, and M. F. Gonzalez-Zalba, "Cmos on-chip thermometry at deep cryogenic temperatures," Applied Physics Reviews **11** (2024).

[15]K. Triantopoulos, M. Cassé, S. Barraud, S. Haendler, E. Vincent, M. Vinet, F. Gaillard, and G. Ghibaudo, "Self-heating effect in fdsoi transistors down to cryogenic operation at 4.2 k," IEEE Transactions on Electron Devices **66**, 3498–3505 (2019).

[16]A. A. Artanov, E. A. Gutiérrez-D, A. R. Cabrera-Galicia, A. Kruth, C. Degenhardt, D. Durini, J. Méndez-V, and S. Van Waasen, "Self-heating effect in a 65 nm mosfet at cryogenic temperatures," IEEE Transactions on Electron Devices **69**, 900–904 (2022).

[17]J. Chawner, S. Barraud, M. Gonzalez-Zalba, S. Holt, E. Laird, Y. A. Pashkin, and J. Prance, "Nongalvanic calibration and operation of a quantum dot thermometer," Physical Review Applied **15**, 034044 (2021).

[18]M. de Kruijf, G. M. Noah, A. Gomez-Saiz, J. J. Morton, and M. F. Gonzalez-Zalba, "Measurement of cryoelectronics heating using a local quantum dot thermometer in silicon," Chip , 100097 (2024).

[19]S. K. Singh, D. Sharma, P. Srinivasan, and A. Dixit, "Quantum-dot-based thermometry using 12-nm finfet and machine learning models," IEEE Transactions on Electron Devices (2024).

[20]A. Y. Choi, I. Esho, B. Gabritchidze, J. Kooi, and A. J. Minnich, "Characterization of self-heating in cryogenic high electron mobility transistors using schottky thermometry," Journal of Applied Physics 130 (2021).

[21]R. Bebitov, O. Abdulkhaev, D. Yodgorova, D. Istamov, G. Khamdamov, S. M. Kuliyev, A. Khakimov, and A. Rakhmatov, "Dependence of the accuracy of the silicon diode temperature sensors for cryogenic thermometry on the spread of their parameters," Low Temperature Physics 49, 256–260 (2023).

[22]J. Qu, S. Benz, H. Rogalla, W. Tew, D. White, and K. Zhou, "Johnson noise thermometry," Measurement Science and Technology 30, 112001 (2019).

[23]A. Casey, F. Arnold, L. V. Levitin, C. P. Lusher, J. Nyéki, J. Saunders, A. Shibahara, H. Van Der Vliet, B. Yager, D. Drung, et al., "Current sensing noise thermometry: a fast practical solution to low temperature measurement," Journal of Low Temperature Physics 175, 764–775 (2014).

[24]Y. S. Ivashchenko, Y. G. Korobchenko, and T. Bondarenko, "Electron temperature of a hydrocarbon flame," Combustion, Explosion and Shock Waves 11, 703–707 (1975).

[25]H. Brixy and T. Kakuta, "Noise thermometer (jaeri review 96-003)," Tokaimura: Japan Atomic Energy Research Institute (1996).

[26]D. Rothfuss, A. Reiser, A. Fleischmann, and C. Enss, "Noise thermometry at ultra-low temperatures," Philosophical Transactions of the Royal Society A: Mathematical, Physical and Engineering Sciences 374, 20150051 (2016).

[27]B. M. Wilamowski and J. D. Irwin, Fundamentals of industrial electronics (CRC Press, 2018) Chap. 11.

[28]J. B. Johnson, "Thermal agitation of electricity in conductors," Physical review 32, 97 (1928).

[29]H. Nyquist, "Thermal agitation of electric charge in conductors," Physical review 32, 110 (1928).

[30]T.-M. Chen and A. Van Der Ziel, "Hanbury brown—twiss type circuit for measuring small noise signals," Proceedings of the IEEE 53, 395–395 (1965).

[31]S. Wolff, "On the brown-twiss circuit," Proceedings of the IEEE 53, 1140–1141 (1965).

[32]E. Rubiola and V. Giordano, "On the 1/f frequency noise in ultra-stable quartz oscillators," in 2006 IEEE International Frequency Control Symposium and Exposition (IEEE, 2006) pp. 759–766.

[33]D. R. White, S. Benz, J. Labenski, S. W. Nam, J. Qu, H. Rogalla, and W. L. Tew, "Measurement time and statistics for a noise thermometer with a synthetic-noise reference," Metrologia 45, 395 (2008).

[34]M. Deen, S. Rumyantsev, and J. Orchard-Webb, "Low frequency noise in heavily doped polysilicon thin film resistors," Journal of Vacuum Science & Technology B: Microelectronics and Nanometer Structures Processing, Measurement, and Phenomena 16, 1881–1884 (1998).

[35]J. Crossno, X. Liu, T. A. Ohki, P. Kim, and K. C. Fong, "Development of high frequency and wide bandwidth johnson noise thermometry," Applied Physics Letters 106 (2015).

[36]Z. Wang, M. Povolotskyi, and D. Vasileska, "Modeling thermal effects for 28-nm node fully depleted soi devices under cryogenic temperatures," IEEE Transactions on Electron Devices (2024).

[37]D. W. Hahn and M. N. Özisik, Heat conduction (John Wiley & Sons, 2012).

[38]A. Savin, J. P. Pekola, D. Averin, and V. Semenov, "Thermal budget of superconducting digital circuits at subkelvin temperatures," Journal of applied physics 99 (2006).

[39]L. C. Camenzind, S. Geyer, A. Fuhrer, R. J. Warburton, D. M. Zumbühl, and A. V. Kuhlmann, "A hole spin qubit in a fin field-effect transistor above 4 kelvin," Nature Electronics 5, 178–183 (2022).

[40]C. H. Yang, R. Leon, J. Hwang, A. Saraiva, T. Tanttu, W. Huang, J. Camirand Lemyre, K. W. Chan, K. Tan, F. E. Hudson, et al., "Operation of a silicon quantum processor unit cell above one kelvin," Nature 580, 350–354 (2020).

[41]L. Petit, J. Boter, H. Eenink, G. Droulers, M. Tagliaferri, R. Li, D. Franke, K. Singh, J. Clarke, R. Schouten, et al., "Spin lifetime and charge noise in hot silicon quantum dot qubits," Physical review letters 121, 076801 (2018).

[42]L. Petit, H. Eenink, M. Russ, W. Lawrie, N. Hendrickx, S. Philips, J. Clarke, L. Vandersypen, and M. Veldhorst, "Universal quantum logic in hot silicon qubits," Nature 580, 355–359 (2020).

[43]W. Albrecht, J. Moers, and B. Hermanns, "Hnf-helmholtz nano facility," Journal of large-scale research facilities JLSRF 3, A112–A112 (2017).

[44]T. Nguyen, A. Tavakoli, S. Triqueneaux, R. Swami, A. Ruhtinas, J. Gradel, P. Garcia-Campos, K. Hasselbach, A. Frydman, B. Piot, et al., "Niobium nitride thin films for very low temperature resistive thermometry," Journal of Low Temperature Physics 197, 348–356 (2019).

[45]O. Bourgeois, E. André, C. Macovei, and J. Chaussy, "Liquid nitrogen to room-temperature thermometry using niobium nitride thin films," Review of scientific instruments 77 (2006).